ENGINEERING COMPUTATIONS, VOL. 10, 99–121 (1993)

Feature & Review
ARTICLES

FUNDAMENTAL ISSUES IN FINITE ELEMENT ANALYSES OF LOCALIZATION OF DEFORMATION*

R. DE BORST

Department of Civil Engineering, Delft University of Technology/TNO Building and Construction Research, PO Box 5048, Delft, The Netherlands

L. J. SLUYS

Department of Civil Engineering, Delft University of Technology, PO Box 5048, Delft, The Netherlands

H.-B. MÜHLHAUS

CSIRO Division of Geomechanics, PO Box 54, Mt. Waverley, Victoria, Australia

AND J. PAMIN

Department of Civil Engineering, Delft University of Technology, PO Box 5048, Delft, The Netherlands

ABSTRACT

Classical continuum models, i.e. continuum models that do not incorporate an internal length scale, suffer from excessive mesh dependence when strain-softening models are used in numerical analyses and cannot reproduce the size effect commonly observed in quasi-brittle failure. In this contribution three different approaches will be scrutinized which may be used to remedy these two intimately related deficiencies of the classical theory, namely (i) the addition of higher-order deformation gradients, (ii) the use of micropolar continuum models, and (iii) the addition of rate dependence. By means of a number of numerical simulations it will be investigated under which conditions these enriched continuum theories permit localization of deformation without losing ellipticity for static problems and hyperbolicity for dynamic problems. For the latter class of problems the crucial role of dispersion in wave propagation in strain-softening media will also be highlighted.

KEY WORDS Deformation localization Finite element analyses Continuum models

INTRODUCTION

Localization of deformation refers to the emergence of narrow regions in a structure where all further deformation tends to concentrate (localize), in spite of the fact that the external actions continue to follow a monotonic loading programme. The remaining parts of the structure usually

* Updated version of keynote lecture presented at the Third International Conference on Computational Plasticity: Fundamentals and Applications, Barcelona, April 1992.

0264–4401/93/020099–23$2.00

Received May 1992

unload and behave in an almost rigid manner. The phenomenon has a detrimental effect on the integrity of the structure and often acts as a direct precursor to structural failure. It is observed for a wide range of materials, including rocks, concrete, soils, metals, alloys and polymers, although the scale of localization phenomena in the various materials may differ by some orders of magnitude: the band width is typically less than a millimetre in metals and several metres for crestal faults in rocks.

In this contribution we address the fundamental issue of developing continuum models that admit localization of deformation while preserving well-posedness of the rate boundary value problem. We shall not discuss matters of element performance such as modifying the element formulation to prevent locking in fully developed plastic flow owing to internal constraints[32] or adding shape functions that facilitate capturing sharp strain gradients[36,50]. These improvements are also vital for properly capturing localization, but even for the 'best element' the resulting numerical model lacks physical significance if the mathematical structure of the continuum model is such that the rate boundary value problem is not well-posed.

We begin with an outline of uniqueness and stability conditions for non-linear boundary value problems of standard (Boltzmann) continua. Particular emphasis is directed towards critical conditions which entail a change of type of the differential problem. Later, we concern ourselves with simple, physically motivated generalizations of the standard continuum theory. Our aim is to obtain a formulation that does not exhibit the difficulties associated with a change of type of the differential equations as occurs in the standard continuum upon the introduction of strain softening. The potential of the new models is demonstrated in numerical analyses of static and dynamic boundary value problems.

MATERIAL INSTABILITY AND LOCALIZATION

Material instabilities

From a mechanical point of view the driving forces behind localization phenomena are material instabilities, that is, the constitutive relationship violates the stability criterion[18,26] that the inner product of the stress rate $\dot{\sigma}$ and the strain rate $\dot{\varepsilon}$ is positive*

$$\dot{\varepsilon}^{\mathrm{T}}\dot{\sigma} > 0 \tag{1}$$

Obviously, this inner product becomes negative when, in a uniaxial tension or compression test, the slope of the homogenized axial stress–axial strain curve is negative. We call this phenomenon *strain softening*. By using the terminology 'homogenized' we refer to the fact that initial flaws and boundary conditions necessarily induce a non-homogeneous stress state in a specimen during testing. In particular during progressive failure of the specimen these flaws and local stress concentrations will cause strongly inhomogeneous deformations of the specimen. The procedure that is normally utilized to derive stress–strain relations, namely dividing the force by the virgin load-carrying area and dividing the displacement of the end of the specimen by the original length so as to obtain stress and strain respectively then no longer reflects what happens at a micro-level and loses physical significance. Nonetheless, we can still use this procedure in a continuum description *provided* that we account for these micro-structural changes by including additional terms in the model.

*The notion of *stability* is not well-defined in the mechanics literature. Indeed, as pointed out by Koiter[21], stability in the sense of Lyapunov, that is loosely stated a finite disturbance of the data of the boundary value problem results in a finite change of its solution, can be proven to be identical with the above definition of stability for *elastic* materials only. For *inelastic* materials there exist other definitions of stability in the literature. Considering purely mechanical processes, i.e. not taking into account heat flow, the authors favour the above definition to the one by Drucker[16].

There is also a class of material instabilities that can cause the inner product of stress rate and strain rate to become negative even without the occurrence of strain softening as defined above. These instabilities can arise when the predominant load-carrying mechanism of the material is due to frictional effects such as in sands, rock joints and in pre-cracked concrete. At a phenomenological level such material behaviour usually results in constitutive models which, in a multiaxial context, have a non-symmetric relation between the stress-rate tensor and the strain-rate tensor. This lack of symmetry is in itself sufficient to cause loss of material stability, even if the slope of the axial stress–strain curve is still rising[40].

The above discussion suggests that material instabilities can be classified into two major categories. In category one the prevailing failure mechanism is decohesion and in the second category failure is governed by (frictional) slip. The first class would then include fracture in masonry, concrete and rocks under low confining pressure levels. Such failures may be denoted as mode-I fracture. The second category encompasses slip processes in metals, soils, and in concrete and rocks under high confining pressure levels (mode-II failure). In the remainder of this article we shall show that this distinction has deep implications for the effectiveness of the various approaches that are used to restore well-posedness of the rate boundary value problem (often referred to as regularization methods).

Mathematical implications

Limiting the discussion to incrementally-linear stress–strain relations, that is the relation between stress rate $\dot{\boldsymbol{\sigma}}$ and strain rate $\dot{\boldsymbol{\varepsilon}}$ can be written as:

$$\dot{\boldsymbol{\sigma}} = \mathbf{D}\dot{\boldsymbol{\varepsilon}} \tag{2}$$

with $\mathbf{D}$ the material tangential stiffness matrix, inequality (1) can be formulated as:

$$\dot{\boldsymbol{\varepsilon}}^{\mathrm{T}}\mathbf{D}\dot{\boldsymbol{\varepsilon}} > 0 \tag{3}$$

The limiting case that the inequality of (3) is replaced by an equality, marks the onset of material instability. Mathematically, this is associated with loss of positive-definiteness of the material tangential stiffness matrix $\mathbf{D}$:

$$\det(\mathbf{D} + \mathbf{D}^{\mathrm{T}}) = 0 \tag{4}$$

Material instability can lead to structural instability. For a structure that occupies a volume V Hill's definition[18] guarantees stability if:

$$\int_V \dot{\boldsymbol{\varepsilon}}^{\mathrm{T}}\dot{\boldsymbol{\sigma}}\,\mathrm{d}V > 0 \tag{5}$$

for all kinematically admissible $\dot{\boldsymbol{\varepsilon}}$. A discrete mechanical system then attains the limiting case of a neutrally stable equilibrium (loss of positive-definiteness of $\mathbf{K}$) if[6,17]:

$$\det(\mathbf{K} + \mathbf{K}^{\mathrm{T}}) = 0 \tag{6}$$

where $\mathbf{K}$ is the structural stiffness matrix,

$$\mathbf{K} = \int_V \mathbf{B}^{\mathrm{T}}\mathbf{D}\mathbf{B}\,\mathrm{d}V \tag{7}$$

In (7) $\mathbf{B}$ is the matrix that relates the strain rate $\dot{\boldsymbol{\varepsilon}}$ to the nodal velocity vector $\dot{\mathbf{a}}$:

$$\dot{\boldsymbol{\varepsilon}} = \mathbf{B}\dot{\mathbf{a}} \tag{8}$$

If the material tangential operator **D** locally loses positive-definiteness, the structural tangential stiffness matrix **K** may cease to be positive-definite as well. Accordingly, the mere existence of material instabilities (e.g. strain softening) may lead to structural instability, even in the absence of geometric destabilizing terms. In itself loss of positive-definiteness of **K** does not explain the frequently reported bizarre results of finite element computations for constitutive models where positive-definiteness of **D** fails at some stage of the loading process. For example, finite element computations of instability phenomena in thin shells, where the destabilization is purely caused by geometrical non-linearity, result in perfectly meaningful results in spite of the fact that (6) is satisfied at some stage of the loading process.

The crucial consequence of the loss of positive-definiteness of the material tangent operator **D** is therefore *not* that it may cause loss of structural stability, but that it may result in *loss of ellipticity* of the equilibrium rate equations. Ellipticity is a necessary condition for well-posedness of the rate boundary value problem, in the sense that a finite number of linearly independent solutions are admitted, continuously depending on the data and not involving discontinuities[4]. Mathematically, loss of ellipticity occurs if:

$$\det(n_j D_{ijkl} n_l) = 0 \tag{9}$$

where the summation convention with respect to repeated indices has been adopted. Physically, condition (9) indicates the existence of a discontinuity (with the normal vector **n**) in the velocity gradient and is coincident with Hill's condition for the propagation of plane acceleration waves in solids[19].

Assuming small displacement gradients loss of material stability as expressed by (4) is a necessary condition for loss of ellipticity. To show this we first substitute the strain rate field that derives from a piecewise homogeneous deformation[5,20,52]:

$$\dot{\varepsilon}_{ij} = \tfrac{1}{2}(n_i m_j + n_j m_i) \tag{10}$$

with **m** an arbitrary vector, in the condition for loss of material stability, i.e. $\dot{\boldsymbol{s}}^{\mathrm{T}}\mathbf{D}\dot{\boldsymbol{\varepsilon}} = 0$, so that $m_i n_j D_{ijkl} m_k n_l = 0$. This identity holds for arbitrary **m** if and only if:

$$\det(\tfrac{1}{2} n_j (D_{ijkl} + D_{klij}) n_l) = 0 \tag{11}$$

Because the real-valued eigenspectrum of $n_j D_{ijkl} n_l$ is bounded by the minimum and maximum eigenvalues of $\frac{1}{2} n_j (D_{ijkl} + D_{klij}) n_l$, $\det(\frac{1}{2} n_j (D_{ijkl} + D_{klij}) n_l)$ always vanishes prior to satisfaction of (9). Since (11) can only be satisfied if material stability is lost ((4)), it follows that loss of ellipticity can only occur if we have loss of material stability.

It is emphasized that ellipticity is a local condition and is but one of the three conditions that are necessary for well-posedness of the rate boundary value problem[4]. The other two conditions for well-posedness are satisfaction of the boundary complementing condition, which excludes the emergence of stationary surface waves (Rayleigh waves), and the satisfaction of the interfacial complementing condition, which excludes the emergence of stationary interfacial waves (Stonely waves)[35].

Before proceeding to a discussion of the various enhancements of the standard, rate-independent continuum we shall briefly recall a third notion that has relevance in analyses of structural failure. When carrying out post-failure computations it is of utmose importance to know whether the post-peak equilibrium path is the most critical in the sense that at the same load level there do not exist alternative equilibrium states at a lower energy level. Put differently, there must be uniqueness of the solution of the incremental boundary value problem. Suppose now that uniqueness of the solution is violated. Then, there must be two different stress rates

$\dot{\sigma}_A$ and $\dot{\sigma}_B$ which both satisfy incremental equilibrium:

$$\int_V \delta\varepsilon^T \dot{\sigma}\, dV = \delta \mathbf{a}^T \dot{\mathbf{f}} \tag{12}$$

where the δ-symbol denotes the variation of a quantity and $\mathbf{f}$ assembles the external actions. Subtraction of both equilibrium equations results in:

$$\int_V \delta\varepsilon^T \Delta\dot{\sigma}\, dV = 0 \tag{13}$$

where the Δ-symbol denotes the difference between two quantities. Introducing the **B**-matrix (cf. (8)), substituting the rate stress–strain relation (2) for both admissible stress rate distributions, and requiring that the result holds for any virtual displacement field $\delta\mathbf{a}$, we observe that multiple solutions will exist if and only if:

$$\mathbf{K}\Delta\dot{\mathbf{a}} = \mathbf{0} \tag{14}$$

with **K** as defined in (7). Condition (14) is satisfied non-trivially if and only if[7]:

$$\det(\mathbf{K}) = 0 \tag{15}$$

Apparently the notions of loss of stability and loss of uniqueness coincide for a symmetric material tangential operator **D**. For non-symmetric operators this is not true. Then loss of stability ($\det(\mathbf{K} + \mathbf{K}^T) \leqslant 0$) may precede loss of uniqueness ($\det(\mathbf{K}) \leqslant 0$) as has first been pointed out by Maier and Hueckel[26].

The above discussion of uniqueness depends heavily on the assumption that for both equilibrium paths the stress rates are related to the strain rates by the same material tangential stiffness matrix. For elasto-plastic solids this is not necessary, since the most critical case may occur if in some parts of the structure that is already in a plastic state, the elastic (unloading) modulus is substituted in the relation between stress rate and strain rate. However, Hill[18] has proved that the case that the elasto-plastic (loading) modulus is substituted for the relation between stress rate and strain rate in the entire plastified area is always the most critical for assessing uniqueness if **D** is symmetric. This proof can be extended to discrete mechanical systems[9]

LOCALIZATION UNDER QUASI-STATIC LOADING CONDITIONS

Loss of well-posedness of the rate boundary value problem results in many undesirable properties of finite element solutions. One of the most striking observations is the complete dependence on the discretization, not only with respect to mesh refinement, but also with respect to mesh alignment. Loss of ellipticity causes the failure zone (crack band, shear zone, crestal fault) to exhibit an extreme tendency to propagate along the mesh lines[33,39,47]. Not all enhancements of the classical, rate-independent continuum are as effective in eliminating this undesirable behaviour. Below we shall examine, by means of numerical experiments, the strong points and weaknesses of the various approaches. Specifically we shall address the issues of a proper formulation of the additional boundary conditions that are required in non-standard continuum theories, the effectiveness of the enhancements when the mesh is refined and/or when the direction of the grid lines is changed (mesh alignment), the difficulties in implementing the model and the conditions under which the model can be used (static vs. transient loadings, mode-I vs. mode-II failure).

The non-local concept

Restricting attention to flow theories of plasticity and small deformation gradients, and neglecting body forces the elasto-plastic rate problem is completely defined by the equilibrium condition:

$$\mathbf{L}^{\mathrm{T}}\dot{\boldsymbol{\sigma}} = \mathbf{0} \tag{16}$$

the kinematic relation:

$$\dot{\boldsymbol{\varepsilon}} = \mathbf{L}\dot{\mathbf{u}} \tag{17}$$

and a set of constitutive equations:

$$\dot{\boldsymbol{\varepsilon}} = \dot{\boldsymbol{\varepsilon}}^e + \dot{\boldsymbol{\varepsilon}}^p \tag{18}$$

$$\dot{\boldsymbol{\varepsilon}}^e = [\mathbf{D}^e]^{-1}\dot{\boldsymbol{\sigma}} \tag{19}$$

$$\dot{\boldsymbol{\varepsilon}}^p = \dot{\lambda}\mathbf{m} \tag{20}$$

subject to the constraints:

$$f \leqslant 0, \qquad \dot{\lambda} \geqslant 0, \qquad f\dot{\lambda} = 0 \tag{21}$$

In (16)–(21) $\boldsymbol{\sigma}$ is a vector that contains the stress components, e.g. $\boldsymbol{\sigma} = (\sigma_{xx}, \sigma_{yy}, \sigma_{zz}, \sigma_{xy})$ for a two-dimensional configuration and $\mathbf{L}$ is a differential operator matrix, which, for the two-dimensional case, is conveniently defined as:

$$\mathbf{L}^{\mathrm{T}} = \begin{bmatrix} \dfrac{\partial \cdot}{\partial x} & 0 & 0 & \dfrac{\partial \cdot}{\partial y} \\ 0 & \dfrac{\partial \cdot}{\partial y} & 0 & \dfrac{\partial \cdot}{\partial x} \end{bmatrix} \tag{22}$$

The strain components, assembled in the vector $\boldsymbol{\varepsilon} = (\varepsilon_{xx}, \varepsilon_{yy}, \varepsilon_{zz}, \varepsilon_{xy})$ are related to the displacement vector $\mathbf{u} = (u_x, u_y)$ by the matrix $\mathbf{L}$ as indicated in (17). The total strain rate $\dot{\boldsymbol{\varepsilon}}$ is additively decomposed into an elastic part $\dot{\boldsymbol{\varepsilon}}^e$ and a plastic part $\dot{\boldsymbol{\varepsilon}}^p$. Between the elastic strain rate and the stress rate we assume the bijective relationship (19), with $\mathbf{D}^e$ the elastic stiffness matrix. The direction of the plastic flow $\dot{\boldsymbol{\varepsilon}}^p$ is determined by the vector $\mathbf{m}$ and its magnitude by the multiplier $\dot{\lambda}$, which follows from the requirement that during continued plastic yielding the stress point must remain on the yield surface $f = 0$. Otherwise, that is if $f < 0$, $\dot{\lambda} = 0$.

In standard plasticity theories, the yield function f depends on the stress tensor $\boldsymbol{\sigma}$, and on a finite number of internal variables, conveniently collected in a vector $\mathbf{q}$: $f = f(\boldsymbol{\sigma}, \mathbf{q})$. For the case of isotropic hardening/softening, to which we shall limit the treatment for sake of simplicity, we have only one internal variable, namely γ^p, thus

$$f = f(\boldsymbol{\sigma}, \gamma^p) \tag{23}$$

with $\gamma^p = \int \dot{\gamma}^p \, \mathrm{d}t$, $\dot{\gamma}$ being an invariant measure of the plastic strain tensor, e.g.,

$$\dot{\gamma}^p = \sqrt{\tfrac{2}{3}(\dot{\boldsymbol{\varepsilon}}^p)^{\mathrm{T}}\dot{\boldsymbol{\varepsilon}}^p} \tag{24}$$

The deficiency of standard rate-independent plasticity theories is that material instability can cause loss of ellipticity. The ensuing loss of well-posedness of the rate boundary value problem then renders numerical results meaningless. Bazant and Lin[3] have suggested to average $\dot{\gamma}^p$, such

that:

$$\bar{\dot{\gamma}}^p = \frac{1}{V_r(\mathbf{x})} \int_V g(\mathbf{s}) \dot{\gamma}^p(\mathbf{x}+\mathbf{s})\, \mathrm{d}V \tag{25}$$

with $V_r(\mathbf{x}) = \int g(\mathbf{s}-\mathbf{x})\, \mathrm{d}V$ and $g(\mathbf{s})$ a weighting function, for which the error function is usually substituted, and to make f dependent on $\bar{\gamma}^p$ in lieu of on γ^p itself:

$$f = f(\boldsymbol{\sigma}, \bar{\gamma}^p) \tag{26}$$

Alternatively, one may first average the plastic strain rate tensor $\dot{\boldsymbol{\varepsilon}}^p$ and then form $\bar{\dot{\gamma}}^p$ as in (24). Numerical experience indicates that the differences between both approaches are marginal. Either approach can lead to a set of rate equations that remains elliptic after the onset of localization. This holds true for mode-I type failure mechanisms (decohesion) and mode-II type failures (slip). The non-local approach is therefore generally effective in numerical simulations for both types of mechanisms.

An important issue in all higher-order continuum models is the proper formulation of the additional boundary conditions. In contrast to the gradient continuum[1,13,14,31,42] and the Cosserat continuum[28,29,41] which will be discussed hereafter, this issue has not yet been addressed properly for the non-local regularization[2,38].

Another disadvantage that adheres to non-local *plasticity* is the fact that the consistency condition, i.e. $\dot{f} = 0$, results in an integro-differential equation instead of in an algebraic equation that can be solved locally:

$$\mathbf{n}^{\mathrm{T}} \dot{\boldsymbol{\sigma}} + \frac{\partial f / \partial \bar{\gamma}^p}{V_r(\mathbf{x})} \int_V g(\mathbf{s}) \dot{\gamma}^p(\mathbf{x}+\mathbf{s})\, \mathrm{d}V = 0 \tag{27}$$

with

$$\mathbf{n} = \frac{\partial f}{\partial \boldsymbol{\sigma}} \tag{28}$$

the gradient to the yield function f. Using (18), (20) and (24) we can restate (27) as:

$$\dot{\lambda} = \frac{\mathbf{n}^{\mathrm{T}} \mathbf{D}^e \dot{\boldsymbol{\varepsilon}}}{\mathbf{n}^{\mathrm{T}} \mathbf{D}^e \mathbf{m}} + \frac{\partial f / \partial \bar{\gamma}^p}{V_r \mathbf{n}^{\mathrm{T}} \mathbf{D}^e \mathbf{m}} \int_V g(\mathbf{s}) \dot{\lambda}(\mathbf{x}+\mathbf{s}) \alpha(\mathbf{x}+\mathbf{s})\, \mathrm{d}V \tag{29}$$

where it is implied that $\dot{\lambda} = \dot{\lambda}(\mathbf{x})$, $\dot{\boldsymbol{\varepsilon}} = \dot{\boldsymbol{\varepsilon}}(\mathbf{x})$ etc., unless specified otherwise and:

$$\alpha = \sqrt{\tfrac{2}{3} \mathbf{m}^{\mathrm{T}} \mathbf{m}} \tag{30}$$

Now, we consider a one-dimensional continuum for simplicity and we approximate the integral of (29) by a finite sum:

$$\dot{\lambda}_i = (\dot{\lambda}_{\mathrm{local}})_i + \frac{\partial f / \partial \bar{\gamma}^p}{V_r \mathbf{n}^{\mathrm{T}} \mathbf{D}^e \mathbf{m}} \sum_{j=0}^{n} w_j g(s_j) \dot{\lambda}(x_i + s_j) \alpha(x_i + s_j) \tag{31}$$

with:

$$(\dot{\lambda}_{\mathrm{local}})_i = \frac{\mathbf{n}^{\mathrm{T}} \mathbf{D}^e \dot{\boldsymbol{\varepsilon}}}{\mathbf{n}^{\mathrm{T}} \mathbf{D}^e \mathbf{m}} \tag{32}$$

and w_j the weight factors. The issue of the missing boundary comes in clearly when evaluating this sum: $\dot{\lambda}$ is undefined for $x_i + s_j > L$, L being the length of the bar. The numerical difficulty

is also obvious: $\dot{\lambda}(x_i + s_j)$ is yet unknown for $s_j \geqslant 0$. To obtain a proper solution we must carry out an iterative procedure within each global equilibrium iteration:

$$\dot{\lambda}_i^k = (\dot{\lambda}_{\text{local}})_i + \frac{\partial f/\partial \bar{\gamma}^p}{V_r \mathbf{n}^T \mathbf{D}^e \mathbf{m}} \sum_{j=0}^{n} w_j g(s_j) \dot{\lambda}^{k-1}(x_i + s_j) \alpha(x_i + s_j) \tag{33}$$

where the superscript k is the iteration counter.

A simple alternative to the iterative procedure defined by (33) would be to carry out no iterations so that the non-local value $\dot{\lambda}_i$ is approximated according to:

$$\dot{\lambda}_i^k = (\dot{\lambda}_{\text{local}})_i + \frac{\partial f/\partial \bar{\gamma}^p}{V_r \mathbf{n}^T \mathbf{D}^e \mathbf{m}} \sum_{j=0}^{n} w_j g(s_j) \dot{\lambda}_{\text{local}}(x_i + s_j) \alpha(x_i + s_j) \tag{34}$$

Such an averaging procedure has been utilized by Bazant and Lin[3] in their algorithm for non-local plasticity. Unfortunately, omission of an iteration loop in which $\dot{\lambda}_i$ is computed properly in accordance with (3) results in loss of satisfaction of the consistency condition, which makes the algorithm defect, especially for large loading steps, cf. Simo[44].

The numerical difficulty discussed above does *not* occur if *total* stress–strain relations are employed, that is when the strain is not decomposed into elastic and plastic components. An example is the elasticity-based non-local damage model of Pijaudier-Cabot and Bazant[2,38], where the averaging process can be carried out directly with respect to the strains. On the contrary, it seems that for such total relations the non-local approach is computationally more efficient than the gradient models to be discussed next[11]

Grade-n *continua*

Gradient-type regularization methods can be derived from fully non-local models by first expanding the weight function $g(\mathbf{s})$ introduced in (25) in a Taylor series about $\mathbf{s} = \mathbf{0}$ and then carrying out the integration[31]. The result is:

$$\dot{\bar{\gamma}}^p = \dot{\gamma}^p + c_1 \nabla^2 \dot{\gamma}^p + c_2 \nabla \dot{\gamma}^p + \cdots \tag{35}$$

where the coefficients c_1, c_2 depend on the form of the weighting function and the dimension considered. Note that the odd derivates cancel because of the implicit assumption of isotropy. Restricting the treatment to second-order derivatives, the functional dependence on the yield function now becomes:

$$f = f(\boldsymbol{\sigma}, \gamma^p, \nabla^2 \gamma^p) \tag{36}$$

The inclusion of gradients in the constitutive model can also be motivated directly on micro-mechanical grounds, without making contact with non-local models. The gradient terms are then thought to reflect the fact that below a certain size scale the interaction between the microstructural carriers of the deformation is non-local, see for example the review paper by Kubin and Lépinoux[23]. A particularly convincing example of non-local hardening models, based on the interaction of a Frank Read source with dipolar dislocation arrangements, has been given by Kratochvil[22]. Other arguments have been given by Aifantis and his co-workers[1,51], while numerical and analytical solutions involving gradient models have been presented by Coleman and Hodgdon[14], Lasry and Belytschko[24] and Schreyer and Chen[42]. For cementitious materials experimental results which show evolving micro-structures during failure have been given by Van Mier[27].

The numerical problem delineated above that prevents an efficient use of elastoplastic non-local

models in principle also applies to gradient plasticity models. However, gradient plasticity has the distinct advantage that the consistency condition now yields a partial differential equation instead of an integro-differential equation, namely for the yield function of (36):

$$\mathbf{n}^{\mathrm{T}}\dot{\boldsymbol{\sigma}} - h\dot{\lambda} + \bar{c}\nabla^2\dot{\gamma}^p = 0 \tag{37}$$

where h and $\bar{c}$ are defined as:

$$h = -\frac{1}{\dot{\lambda}}\frac{\partial f}{\partial \gamma^p}\dot{\gamma}^p \qquad \bar{c} = \frac{\partial f}{\partial \nabla^2 \gamma^p} \tag{38}$$

If the partial differential equation (37) is, just as the equilibrium condition (16), satisfied in a weak sense only, a set of equations results that is suitable as a starting point for large-scale finite element computations in two and three dimensions:

$$\int_V \delta\dot{\lambda}(\mathbf{n}^{\mathrm{T}}\dot{\boldsymbol{\sigma}} - h\dot{\lambda} + \bar{c}\nabla^2\dot{\gamma}^p)\,\mathrm{d}V = 0 \tag{39a}$$

$$\int_V \delta\dot{\mathbf{u}}^{\mathrm{T}}[\mathbf{L}^{\mathrm{T}}\dot{\boldsymbol{\sigma}}]\,\mathrm{d}V = 0 \tag{39b}$$

In the two-dimensional examples we shall adopt a Drucker–Prager yield function:

$$f = \sqrt{3J_2} + \alpha p - \bar{\sigma}(\gamma^p, \nabla^2\gamma^p) \tag{40}$$

with J_2 the second invariant of the deviatoric stress tensor, p the hydrostatic pressure, α a friction coefficient and $\bar{\sigma}$ reflecting the cohesion of the material. Substituting the yield function (40) into the flow rule (20) and this result subsequently into the strain-hardening hypothesis (24) gives $\dot{\gamma}^p = \dot{\lambda}\sqrt{1 + 2\alpha^2/9}$. With $c = \bar{c}\sqrt{1 + 2\alpha^2/9}$ we now obtain in lieu of (39):

$$\int_V \delta\dot{\lambda}(\mathbf{n}^{\mathrm{T}}\dot{\boldsymbol{\sigma}} - h\dot{\lambda} + c\nabla^2\dot{\lambda})\,\mathrm{d}V = 0 \tag{41a}$$

$$\int_V \delta\dot{\mathbf{u}}^{\mathrm{T}}[\mathbf{L}^{\mathrm{T}}\dot{\boldsymbol{\sigma}}]\,\mathrm{d}V = 0 \tag{41b}$$

Together with the kinematic relation (17) and the elastic stress–strain relation (19), both of which are satisfied in a pointwise manner, (41) completely define the elastoplastic rate boundary value problem. The fact that the consistency condition is no longer satisfied in a pointwise manner marks a major departure from return-mapping algorithms that are used in conventional plasticity. Now, the plastic multiplier $\dot{\lambda}$ is considered as a fundamental unknown and has a role similar to that of the displacements. It is solved for at global level simultaneously with the displacement degrees-of-freedom.

The displacement field $\mathbf{u}$ and the field of plastic multipliers λ can be discretized to nodal variables $\mathbf{a}$ and $\boldsymbol{\Lambda}$ in the usual way, leading to the following set of equations:

$$\begin{bmatrix} \mathbf{K}_{aa} & \mathbf{K}_{a\lambda} \\ \mathbf{K}_{a\lambda}^{\mathrm{T}} & \mathbf{K}_{\lambda\lambda} \end{bmatrix} \begin{bmatrix} \dot{\mathbf{a}} \\ \dot{\boldsymbol{\Lambda}} \end{bmatrix} = \begin{bmatrix} \dot{\mathbf{f}}_e \\ \mathbf{0} \end{bmatrix} \tag{42}$$

where

$$K_{aa} = \int_V \mathbf{B}^{\mathrm{T}}\mathbf{D}^{\mathrm{c}}\mathbf{B}\,\mathrm{d}V \tag{43}$$

$$\mathbf{K}_{a\lambda} = -\int_V \mathbf{B}^T\mathbf{D}^e\mathbf{n}\mathbf{h}^T \, dV \tag{44}$$

$$\mathbf{K}_{\lambda\lambda} = \int_V [(h + \mathbf{n}^T\mathbf{D}^e\mathbf{n})\mathbf{h}\mathbf{h}^T - c\mathbf{h}\mathbf{p}^T] \, dV \tag{45}$$

and $\mathbf{f}_e$ the external force vector. In (42)–(45) $\mathbf{h}^T = [h_1, \ldots, h_n]$ is the vector that contains the interpolation polynomials for the plastic multiplier and $\mathbf{p}^T = [\nabla^2 h_1, \ldots, \nabla^2 h_n]$. The detailed derivation of these equations and the finite elements that have been constructed on the basis of them are described in References 13 and 37.

An unpleasant property of (42) is the unsymmetry that enters through $\mathbf{K}_{\lambda\lambda}$ as defined in (45). For the pure rate problem $\mathbf{K}_{\lambda\lambda}$ can be symmetrized. Introducing $\mathbf{q}^T = [\nabla h_1, \ldots, \nabla h_n]$ and using Green's theorem we obtain:

$$\mathbf{K}_{\lambda\lambda} = \int_V [(h + \mathbf{n}^T\mathbf{D}^e\mathbf{n})\mathbf{h}\mathbf{h}^T + c\mathbf{q}\mathbf{q}^T] \, dV \tag{46}$$

and the non-standard boundary conditions at the elastoplastic boundary S_λ: $\delta\dot{\lambda} = 0$ or $(\nabla\dot{\lambda})^T\mathbf{n}_\lambda = 0$. $\mathbf{n}_\lambda$ is the outward normal at S_λ. These results can also be derived directly from a variational principle[13,31]. Unfortunately, it seems that, when finitely sized loading steps are used, the symmetric form of $\mathbf{K}_{\lambda\lambda}$ does not give a proper convergence behaviour in an incremental-iterative procedure and that one then has to resort to the unsymmetric form of $\mathbf{K}_{\lambda\lambda}$ as in (45).

We shall now illustrate the good performance of the theory in localization problems by two examples. First, a one-dimensional tension bar is studied. *Figure 1* shows the loading configuration and lists the relevant material data. As in all subsequent examples a linear softening branch is adopted. This assumption permits constructing an exact analytical solution for the width w of the localization zone and the slope of the stress–displacement curve when the localization zone has developed fully[13]:

$$w = 2\pi l, \qquad l = \sqrt{-c/h} \tag{47}$$

$$\dot{u}/\dot{\sigma} = L/E + 2\pi l/h \tag{48}$$

For the purpose of fixing the localization zone the elements between $x = 45$ mm and $x = 55$ mm were assigned a reduction of 10% in the initial tensile strength σ_t. Dividing the bar into 20, 40, 80 and 160 elements, respectively, results in a good convergence to the analytical solution, both with respect to the band width (*Figure 2*) and with respect to the stress–displacement curve (left part of *Figure 3*). The right part of *Figure 3* shows the effect of varying the ratio of the internal length scale l over the structural size L. We observe a clear size effect, that is a smaller value of l/L (a smaller internal length scale or a larger structure) results in a more brittle behaviour.

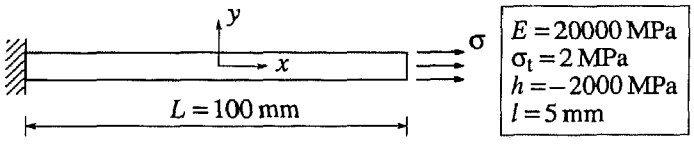

Figure 1 Tension bar with a length L subjected to an axial stress σ

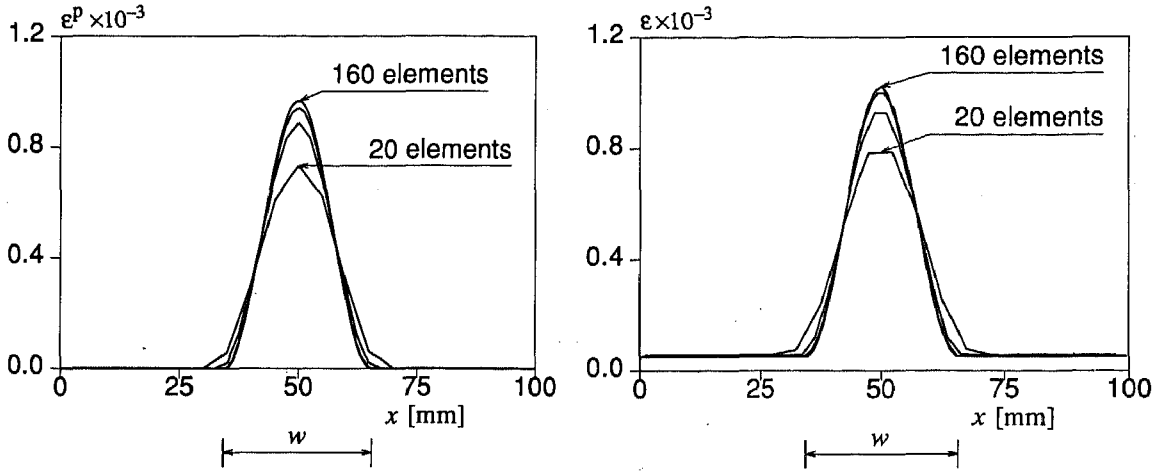

Figure 2 Plastic (left) and total (right) strain distribution along the axis of an imperfect tension bar for different discretizations ($l/L = 0.05$ and $u = 0.02$)

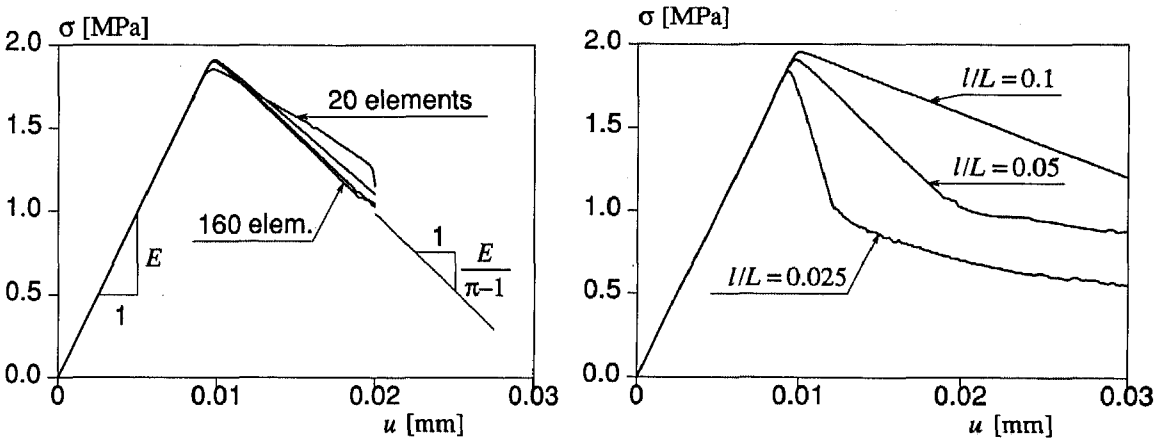

Figure 3 Axial stress vs. axial displacement of right end of a tension bar. Left: results for $l/L = 0.05$ and different discretizations (20, 40, 80 and 160 elements). Right: results for different ratios of l/L (160 elements)

The specimen that has been considered for the biaxial test has a width of 60 mm and height of 180 mm. Smooth boundary conditions ($u_y = 0$) were assumed at the upper and lower boundaries. The additional boundary condition $(\nabla \dot{\lambda})^T \mathbf{n}_\lambda = 0$ was used at all boundaries. A Drucker–Prager gradient plasticity model was used with an associated flow rule and the following material data: Young's modulus $E = 11920$ MPa, Poisson's ratio $\nu = 0.49$, $\alpha = 2/3$, $\bar{\sigma} = 106(1 - 4\gamma^p)$ and $c = 2500$ MPa.

An imperfect element (10% reduction in the cohesion of the element at the left boundary near the horizontal centreline) was used to set the starting point of the shear band development. *Figure 4* shows that initially two shear bands arise, but that later only one shear band persists. The above observation shows that the addition of higher-order gradients does not remove the existence of alternative equilibrium branches (bifurcations points). Indeed, some form of

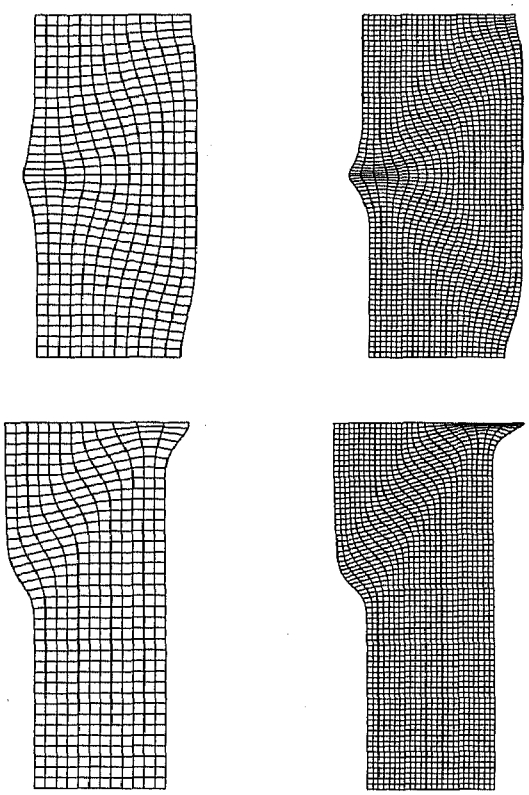

Figure 4 Incremental displacements at peak load (above) and beyond peak load (below). Left: mesh with 432 four-noded elements. Right: mesh with 1728 four-noded elements

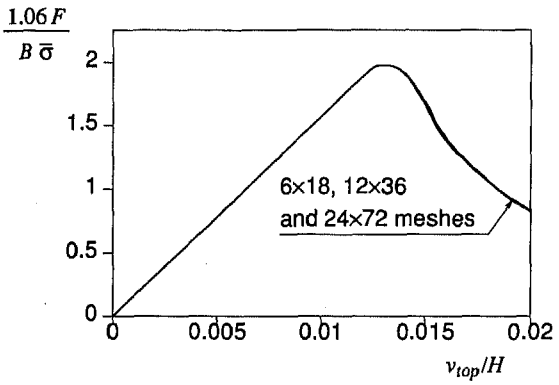

Figure 5 Load–displacement curves for a plane-strain biaxial test. Results for a Drucker–Prager gradient plasticity model and nine-noded elements

geometric non-symmetry—in this case the fact that the imperfect element is not located symmetrically with respect to the upper and lower boundaries—is necessary to trigger the symmetry-breaking solution.

The results shown in *Figure 4* were obtained using a four-noded element with a bilinear interpolation for the displacements and a Hermitian (bicubic) interpolation for the plastic multiplier[37]. Despite the apparent convergence in the failure patterns of *Figure 4*, convergence was not obtained for the load–displacement curves. It seems that this is due to the ill-matched orders of interpolation of the displacements and the plastic multiplier, since a perfect convergence was obtained when the bilinear interpolation for the displacements was replaced by a biquadratic Lagrangean interpolation (*Figure 5*).

In sum, we conclude that gradient plasticity theories are highly versatile for describing localization of deformation in a continuum setting. They can be made effective for mode-I and mode-II failures, in particular if an 'isotropic' dependence on the higher-order deformation gradients is assumed as has been done here via the Laplacian of the internal state variable γ^p. Furthermore, the formulation outlined above can be connected to a variational principle[13,31], which ensures that the issue of the additional, non-standard boundary conditions is addressed properly. A disadvantage of the proposed algorithmic formulation is the introduction of an

additional variable at global level in addition to the conventional displacement degrees-of-freedom.

Cosserat continua

Unlike the non-local and grade-n continuum models the structure of the plasticity formalism is retained in the Cosserat continuum (E. and F. Cosserat[15]) in the sense that the yield function f depends only on the stress tensor and on a *local* internal variable, say γ^p as in (23). The regularizing effect now comes from the introduction of additional static and kinematic quantities, namely the couple-stresses m_{zx} and m_{zy} (*Figure 6*) and the micro-curvatures $\kappa_{zx} = \partial\omega_z/\partial x$ and $\kappa_{zy} = \partial\omega_z/\partial y$ (for a two-dimensional continuum). ω_z is a micro-rotation about the z-axis which in the planar Cosserat theory appears as a third independent kinematic quantity in addition to the two displacement components u_x and u_y. Since these static and kinematic components are related through a 'bending' modulus, and since the quotient of a bending modulus and the conventional Young's modulus has the dimension of length, an internal length scale, say l, is introduced already in the elastic regime. Note that this is not so for the non-local and grade-n continuum models discussed in the preceding sections, where the enrichment is introduced only in the inelastic regime.

In spite of the introduction of new static and kinematic quantities, the whole framework for elastoplasticity as laid down in (16)–(21) can still be used. We merely have to redefine $\mathbf{u}$, $\boldsymbol{\varepsilon}$ and $\boldsymbol{\sigma}$ as:

$$\mathbf{u} = [u_x, u_y, \omega_z]^T \tag{49}$$

$$\boldsymbol{\varepsilon} = [\varepsilon_{xx}, \varepsilon_{yy}, \varepsilon_{zz}, \varepsilon_{xy}, \varepsilon_{yx}, \kappa_{xz}l, \kappa_{yz}l]^T \tag{50}$$

$$\boldsymbol{\sigma} = [\sigma_{xx}, \sigma_{yy}, \sigma_{zz}, \sigma_{xy}, \sigma_{yx}, m_{xz}/l, m_{yz}/l]^T \tag{51}$$

where the internal length scale l has been introduced in (50) and (51) to make all components in $\boldsymbol{\varepsilon}$ and $\boldsymbol{\sigma}$ having the same dimension. The operator matrix $\mathbf{L}$ and the elastic stiffness matrix

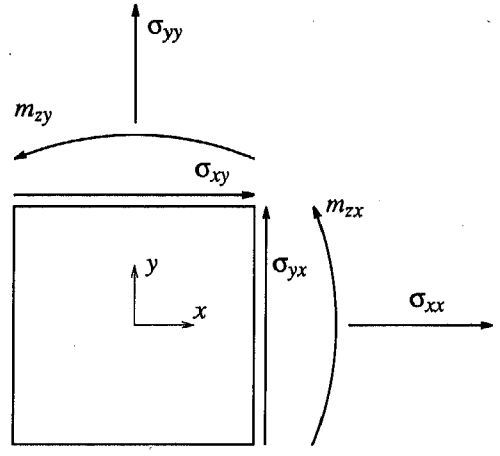

Figure 6 Stress and couple-stress in a two-dimensional Cosserat continuum

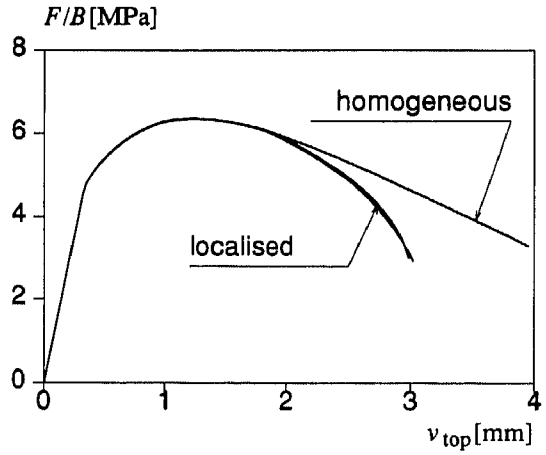

Figure 7 Load–displacement curves for a plane-strain biaxial test (Drucker–Prager Cosserat plasticity)

$\mathbf{D}^e$ and the elastic stiffness matrix $\mathbf{D}^e$ have to be redefined as[8–10,12]:

$$\mathbf{L}^T = \begin{bmatrix} \frac{\partial \cdot}{\partial x} & 0 & 0 & \frac{\partial \cdot}{\partial y} & 0 & 0 & 0 \\ 0 & 0 & 0 & 0 & \frac{\partial \cdot}{\partial x} & 0 & 0 \\ 0 & \frac{\partial \cdot}{\partial y} & 0 & +1 & -1 & l\frac{\partial \cdot}{\partial x} & l\frac{\partial \cdot}{\partial y} \end{bmatrix} \tag{52}$$

and

$$\mathbf{D}^e = \begin{bmatrix} 2\mu c_1 & 2\mu c_2 & 2\mu c_2 & 0 & 0 & 0 & 0 \\ 2\mu c_2 & 2\mu c_1 & 2\mu c_2 & 0 & 0 & 0 & 0 \\ 2\mu c_2 & 2\mu c_2 & 2\mu c_1 & 0 & 0 & 0 & 0 \\ 0 & 0 & 0 & \mu + \mu_c & \mu - \mu_c & 0 & 0 \\ 0 & 0 & 0 & \mu - \mu_c & \mu + \mu_c & 0 & 0 \\ 0 & 0 & 0 & 0 & 0 & 2\mu & 0 \\ 0 & 0 & 0 & 0 & 0 & 0 & 2\mu \end{bmatrix} \tag{53}$$

with $c_1 = (1-\nu)/(1-2\nu)$ and $c_2 = \nu/(1-2\nu)$. The constants μ and ν have the classical meaning of a shear modulus and Poisson's ratio, respectively. μ_c is a rotational shear modulus and completes the total of four constants that are needed to describe the elastic behaviour of an isotropic Cosserat continuum under planar deformations. The coefficient 2 has been introduced in the terms D^e_{66} and D^e_{77} to arrive at a convenient form of the elasto-plastic constitutive equations[9,12]. The total bending stiffness that sets the relation between the micro-curvatures and the couple-stresses is determined by the value of the internal length scale l.

For the extension of the theory to account for plastic flow we merely have to redefine the invariants on which the yield function depends. For example, the invariant J_2 of the deviatoric stress tensor and the hardening parameter γ^p on which the Drucker–Prager yield function:

$$f = \sqrt{3J_2} + \alpha p - \bar{\sigma}(\gamma^p) \tag{54}$$

depends, are generalized as[28]:

$$J_2 = a_1 s_{ij} s_{ij} + a_2 s_{ij} s_{ji} + a_3 m_{ij} m_{ij}/l^2 \tag{55}$$

and

$$\dot{\gamma}^p = [b_1 \dot{e}^p_{ij} \dot{e}^p_{ij} + b_2 \dot{e}^p_{ij} \dot{e}^p_{ji} + b_3 \dot{\kappa}^p_{ij} \dot{\kappa}^p_{ij} l^2]^{1/2} \tag{56}$$

s_{ij} is the deviatoric stress tensor and $\dot{e}^p_{ij}$ is the plastic deviatoric strain-rate tensor. a_1, a_2, a_3 and b_1, b_2, b_3 are material parameters. Based on micromechanical considerations Mühlhaus and Vardoulakis[28] have proposed the values $a_1 = 3/4$, $a_2 = -1/4$ and $a_3 = 1/8$. In the example calculations presented here the values $a_1 = 1/4$, $a_2 = 1/4$ and $a_3 = 1/2$ have been adopted, since these values give rise to a particularly simple algorithm[9]. In order that $\dot{\gamma}^p$ is energetically conjugate to J_2, b_1, b_2 and b_3 must then be assigned the following values: $b_1 = 1/3$, $b_2 = 1/3$ and $b_3 = 2/3$. To bring out the essential features of the Cosserat model the present choice is permissible. When it is attempted to fit the material behaviour as closely as possible this is unlikely to be the case.

To demonstrate the effectiveness of the Cosserat continuum for failure problems where the

prevailing mechanism is frictional sliding the same biaxial test has been considered as in the previous section. Natural boundary conditions for the rotations were assumed at all sides (ω_z free). A Drucker–Prager yield function was employed with a non-associated (plastically incompressible) flow rule and the following material data: Young's modulus $E = 2400$ MPa, Poisson's ratio $\nu = 0.2$, $\mu_c = 500$ MPa, $l = 6$ mm, $\alpha = 1.2$, $\bar{\sigma} = 1.2\sqrt{3}(1 - 25\gamma^p)$. The load–deflection curves for all three discretizations (108, 432 and 1728 six-noded triangular elements respectively) are shown in *Figure 7* together with the solution that is obtained under the assumption of homogeneous deformations (no localization). As with the gradient model an imperfect element at the left boundary near the horizontal centreline was used to set the starting point of the shear band development. Again, two shear bands arise initially, but finally only one shear band persists (*Figure 8*).

Mühlhaus and Vardoulakis[27] were the first to recognize that the Cosserat approach introduces a length scale in the continuum description and that the rate boundary value problem remains elliptic after the onset of shear banding. Finite element analyses showing convergence to a physically realistic solution have been presented by de Borst[9,12] and Mühlhaus *et al.*[30]. The approach has several advantages, especially from a numerical point of view. If the incremental stress–strain relation is symmetric, the structural tangent stiffness matrix also remains symmetric, which is not the case for the non-local and not necessarily so for grade-n continua. Further, no special algorithms are necessary as the return-mapping algorithms used in standard plasticity can be carried over to Cosserat elastoplasticity in a straightforward fashion and the standard procedure for deriving consistent tangent operators can still be applied[9,12]. A distinct disadvantage of the Cosserat continuum is that it is only effective as a regularization method if grain boundary sliding is the dominant carrier of the inelastic deformation (mode-II failures). Indeed, already in cases that we do not have pure shear, as for the biaxial test considered above, the regularization mechanism is often weak. Then, it may happen that the deficiencies of the classical continuum are remedied only partly. For instance, Sluys[47] has shown that for such a specimen there is convergence to a unique, physically realistic solution upon mesh refinement, but that the solution heavily depends on the direction of the mesh lines (mesh alignment). A further disadvantage is that the rotations emerge as additional degrees-of-freedom at global level, which increases the computational effort.

LOCALIZATION UNDER DYNAMIC LOADING CONDITIONS

All higher-order continua as well as rate-dependent continuum models share the property that, unlike the standard, rate-independent continuum, wave propagation becomes dispersive, that is, waves with different wave numbers propagate with different velocities and, consequently, the shape of a pulse is altered during propagation. This is of crucial importance when modelling localization under dynamic loading conditions.

Cosserat continua

Since the enhancement of Cosserat continuum over the classical continuum is present during elastic and inelastic deformations wave propagation already becomes dispersive in the elastic region. This is clearly shown in *Figure 10* for a shear stress wave which propagates in the shear layer of *Figure 9*. Assuming purely elastic material behaviour we observe that an initially linear wave front gradually transforms when the wave propagates through the layer.

This behaviour will now be investigated by carrying out a dispersion analysis in the elastic

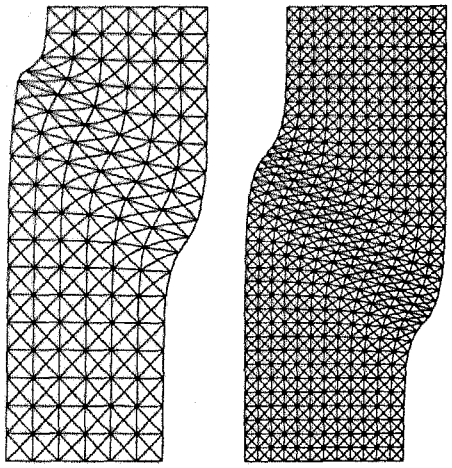

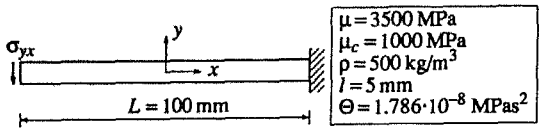

Figure 9 Bar in pure shear with a length L subjected to a transverse stress σ_{yx}

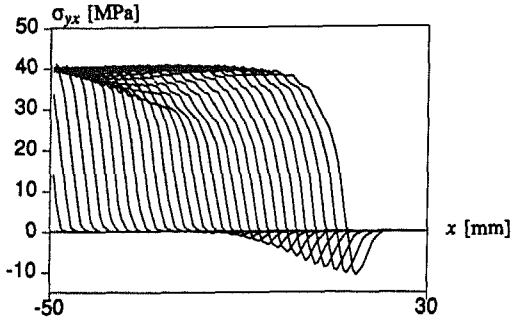

Figure 8 Incremental displacements for a plane-strain biaxial test (Drucker–Prager Cosserat plasticity)

Figure 10 Wave propagation in a shear layer of an elastic Cosserat material

domain. For the shear layer of *Figure 9* the governing equations are given by[10]

$$(\mu + \mu_c)\frac{\partial^2 u_y}{\partial x^2} - 2\mu_c \frac{\partial \omega_z}{\partial x} = \rho \frac{\partial^2 u_y}{\partial t^2} \tag{57}$$

$$2\mu l^2 \frac{\partial^2 \omega_z}{\partial x^2} + 2\mu_c \frac{\partial u_y}{\partial x} - 4\mu_c \omega_z = \Theta \frac{\partial^2 \omega_z}{\partial t^2} \tag{58}$$

where ρ is the density and Θ is the inertia of micro-rotation per unit volume. We consider waves which propagate in the x-direction with wave number k and angular frequency ω. A general solution for u_y and ω_z of the form:

$$u_y(x, t) = A_1 \exp(i(kx - \omega t)) \tag{59}$$

$$\omega_z(x, t) = A_2 \exp(i(kx - \omega t)) \tag{60}$$

is now assumed. Substitution of this solution in (57)–(58) yields the dispersion relations for the phase velocity c_f and the group velocity c_g, c_f–k and c_g–k. In *Figure 11* relations are plotted for the shear wave and for the micro-rotation wave, which is not present in the classical continuum. Using the conditions $u_y = 0$ and $\omega_z = 0$ at both boundaries the exact analytical values of the wave numbers k and the angular frequencies ω can be calculated[47]. It is noted that when an axial stress is applied instead of a shear stress, so that a longitudinal wave propagates in the bar, we do not observe dispersion. This confirms the assertion that the Cosserat continuum is effective as a regularization method only for mode-II failures.

Now, the effect of mesh refinement of the shear layer is investigated for a softening Cosserat plasticity model with a Von Mises yield function ($\alpha = 0$ in (54)). The data listed in *Figure 9* were supplemented by a virgin yield strength $\bar{\sigma}(0) = 100$ MPa and a softening modulus $h = -0.4762\,\mu$. *Figure 12* shows that we obtain convergence to a physically realistic solution, both in terms of the strain profile and in terms of the energy dissipation. For two-dimensional

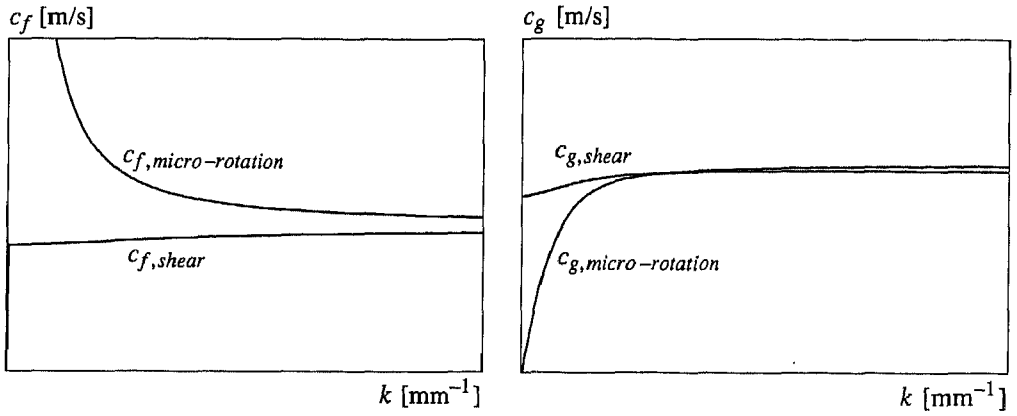

Figure 11 Dispersion relations c_f–k (left) and c_g–k (right) for a shear layer of an elastic Cosserat material

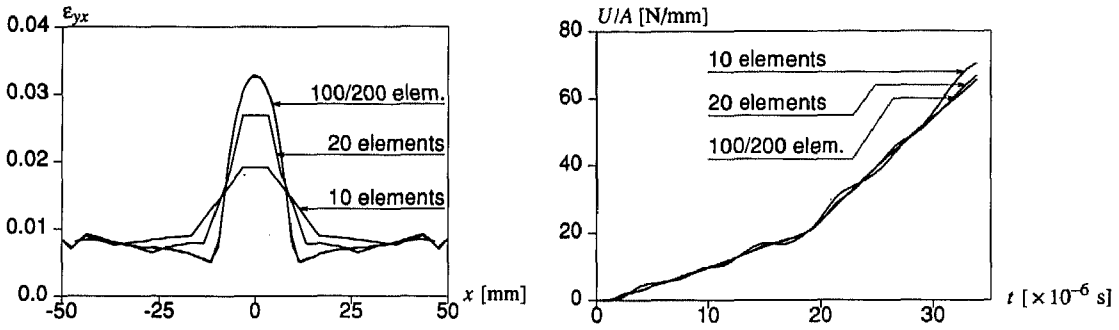

Figure 12 Strain distributions and energy dissipation for impact loading on a shear layer of an elastoplastic Cosserat material

examples with impact loading of strain-softening Cosserat media the reader is referred to de Borst and Sluys[10] and to Sluys[47].

*Grade-*n *continua*

For the gradient model discussed here the enrichment only applies in the inelastic regime. As a consequence dispersion is only present after the onset of plasticity. But in contrast to the Cosserat continuum dispersive waves now also arise for tensile loadings. For the one-dimensional tension bar of *Figure 1* the following differential equation for the axial displacement u describes the wave propagation[46,47]:

$$-hl^2\left(\frac{\partial^4 u}{\partial x^4} - \frac{\rho}{E}\frac{\partial^4 u}{\partial x^2 \partial t^2}\right) + \frac{\rho(E+h)}{E}\frac{\partial^2 u}{\partial t^2} - h\frac{\partial^2 u}{\partial x^2} = 0 \tag{61}$$

Assuming a general solution of the form:

$$u(x,t) = A\exp(ik(x-ct)) \tag{62}$$

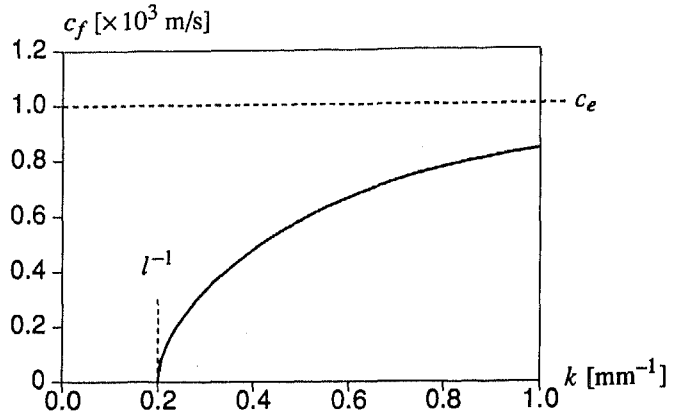

Figure 13 Dispersion relation (c_f–k curve) for gradient-dependent plasticity

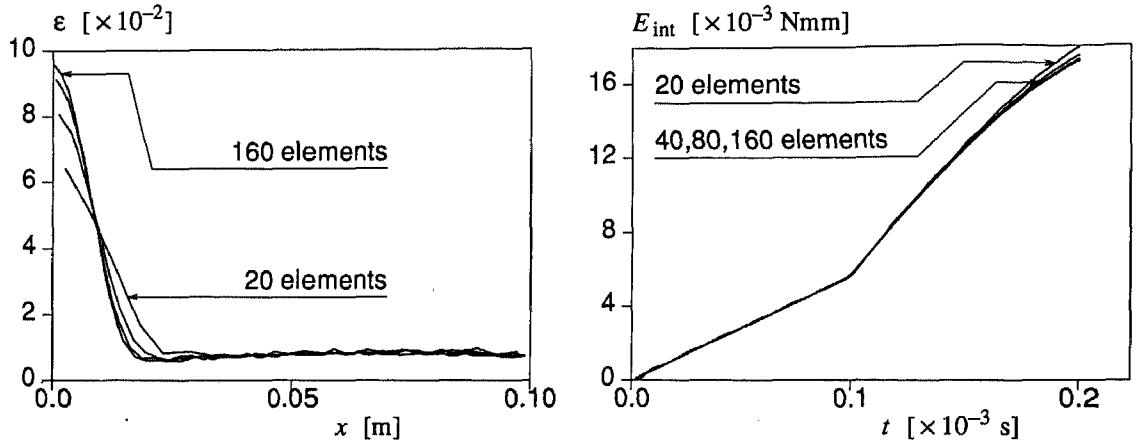

Figure 14 Strain localization (left) and energy consumption (right) in tension bar of gradient material

we arrive at the following dispersion relation between the phase velocity c_f and the wave number k:

$$c_f = c_e((h - hl^2k^2)/(E + h - hl^2k^2))^{1/2} \tag{63}$$

with c_e the elastic wave speed (*Figure 13*). A numerical solution of the tension bar problem is presented in *Figure 14*. The impact loading at the right end of the bar is immediately present with a magnitude of $\sigma = 0.75\,\sigma_t$. The material data are as given in *Figure 1* with in addition $\rho = 2 \times 10^{-8}$ N s^2 mm^{-2}. However, no imperfection is inserted in the model, but the localization starts at the left boundary when the reflection of the tensile wave on this fixed boundary causes a doubling of the stress intensity. Finally, *Figure 15* presents results for a dynamic calculation of a biaxial test with a Drucker–Prager gradient plasticity model with a non-associated (plastically incompressible) flow rule[47]

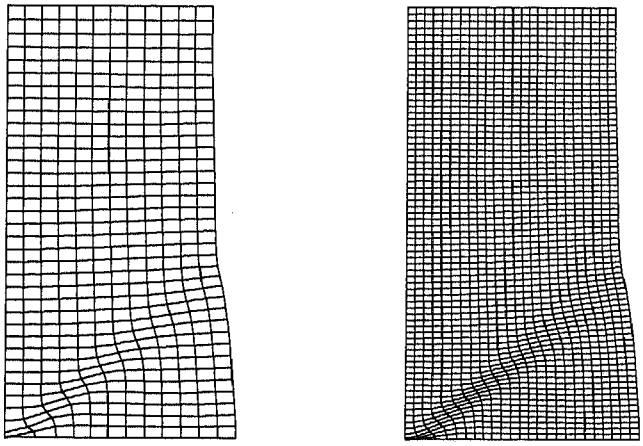

Figure 15 Total displacements caused by impact loading of a biaxial test specimen. A Drucker–Prager gradient model has been used for two discretizations

Rate-dependent continua

Rate-dependence was introduced to describe failure processes in metals by Needleman[34], Shawki and Clifton[43] and Wu and Freund[53]. Later, it was applied to soils by Loret and Prévost[25] and to concrete and rock fracture by Sluys and de Borst[45,47,49]. From a physical point of view the addition of rate dependence is the most appealing solution. It works equally well for both failure mechanisms. For instance, there is no influence of the direction of the mesh lines on the solution[47,48], but its applicability is obviously limited to transient loading conditions and the regularizing effect rapidly decreases for slow loading rates or when we approach the rate-independent limit.

In what follows below the simple linear rate-dependent crack model of Sluys and de Borst[45,47,49] is considered:

$$\sigma = \sigma_t + h\varepsilon^p + m\frac{\partial \varepsilon^p}{\partial t} \tag{64}$$

with m a rate-sensitivity parameter (here taken as $m = 0.2\ \mathrm{Ns/mm^2}$). For the one-dimensional bar of *Figure 1* the governing differential equation reads:

$$m\left(\frac{\rho}{E}\frac{\partial^3 u}{\partial t^3} - \frac{\partial^3 u}{\partial x^2 \partial t}\right) + \frac{\rho(E+h)}{E}\frac{\partial^2 u}{\partial t^2} - h\frac{\partial^2 u}{\partial x^2} = 0 \tag{65}$$

A proper dispersion analysis can now only be carried out if the harmonic waves are attenuated exponentially when propagating through the solid[47,49]:

$$u(x,t) = A\exp((-\alpha + ik)x - i\omega t) \tag{66}$$

The dispersion relations c_f–ω and c_g–ω for the phase velocity c_f and the group velocity c_g respectively that result from this analysis are shown in *Figure 16*. In the right part of *Figure 16* the damping coefficient α is plotted as a function of the angular frequency ω. The limit of α with respect to ω is $\lim_{\omega \to \infty} \alpha(\omega) = l^{-1}$ where $l = 2mc_e/E$ is the internal length scale of the rate-dependent model.

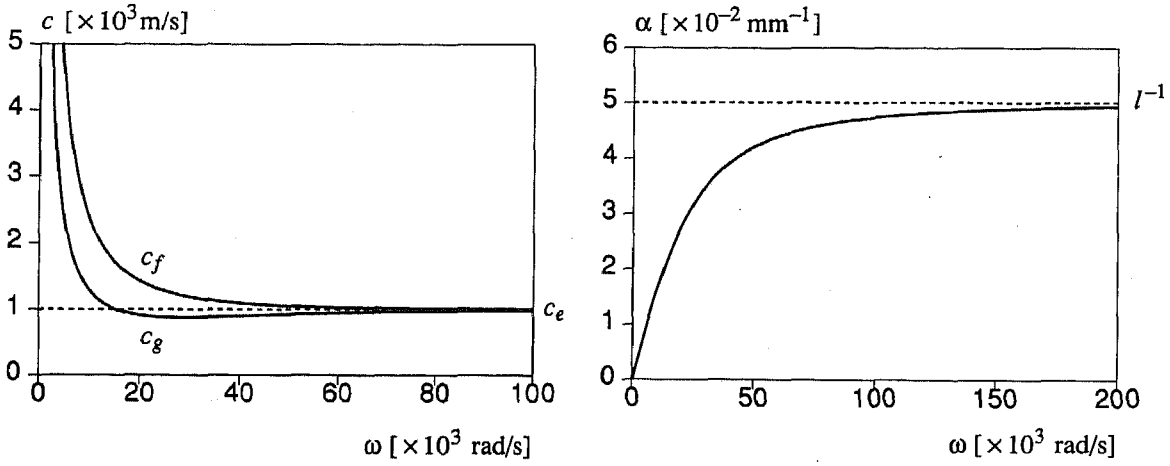

Figure 16 c–ω *and* α–ω curves for a rate-dependent tension bar

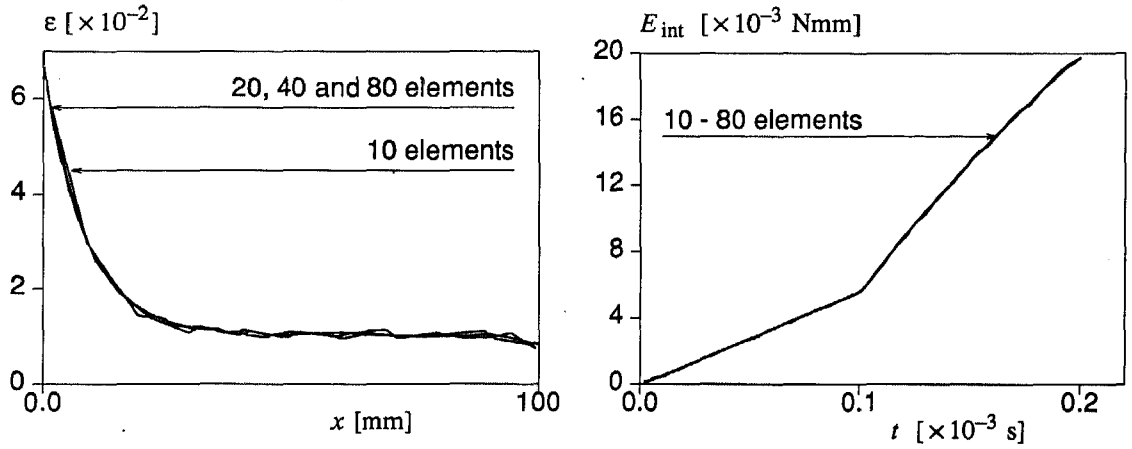

Figure 17 Strain localization (left) and energy consumption (right) for rate-dependent tension bar

A numerical solution of the tension bar problem is given in *Figure 17*. The material data are as for the analysis with the gradient model in the previous section except that now $h = -5000$ MPa. Finally, *Figure 18* shows the development of a shear band in a plane-strain biaxial test with a rate-dependent material. Duvaut–Lions viscoplasticity was used with a Drucker–Prager yield surface and a non-associated (plastically incompressible) flow rule. A symmetric half of the specimen was considered, so that the condition at the left boundary reads: $u_x = 0$. We clearly observe that the shear band runs steeper than the mesh lines, which are under 45°[47,48].

CONCLUDING REMARKS AND OUTSTANDING PROBLEMS

In this contribution an attempt has been made to give an overview of current developments in finite element analysis of localization phenomena. It has been argued that various promising approaches exist, but that there is no such thing like a panacea which cures the shortcomings

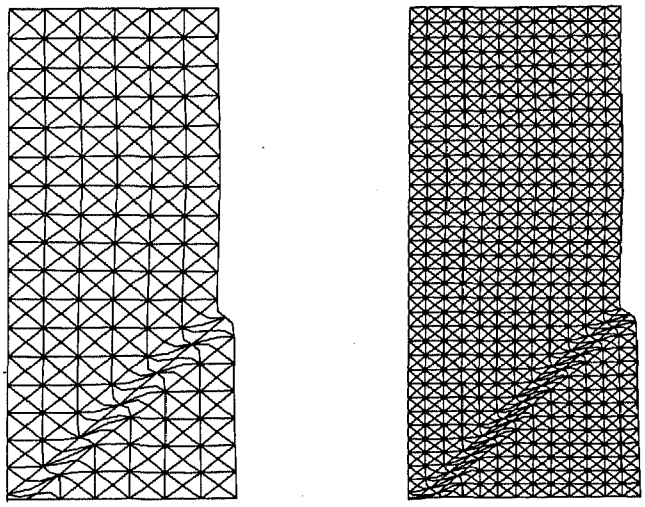

Figure 18 Total displacements caused by impact loading of a biaxial test specimen. A Drucker–Prager viscoplastic model has been used for two discretizations

of standard, rate-independent continua upon the introduction of strain softening and/or non-symmetry in the constitutive rate equations.

No completeness is claimed. This holds true with respect to computational and constitutive aspects that have been touched in this contribution, but above all with respect to outstanding problems which hamper the effective and accurate numerical prediction of the failure and post-failure behaviour of structures. In the authors' opinion the most pressing issues that prohibit the successful use of numerical models in failure computations are:

- The proper determination of the additional model parameters that emerge in the higher-order and rate-dependent continuum models when compared to the classical approach. Especially in higher-order continua this problem is not solved easily, since the additional parameters are *not directly derivable* from elementary tests such as uniaxial or triaxial tension or compression tests. Even if one would be able to carry out a test on a perfect specimen, so that homogeneous deformations would occur throughout the entire loading programme, these parameters could not be measured because for homogeneous deformations there is no effect of the higher-order continuum models. Therefore, one must proceed in a semi-inverse manner, whereby the experimental results of different types of tests are fitted in the post-peak regime.
- The steep (but finite!) strain gradients that occur in higher-order and rate-dependent continua during failure require that very fine meshes are used to capture the failure mode properly. If such analyses are to be carried out on nowadays' or even tomorrow's computers, then the use of adaptive mesh refinement techniques is a *conditio sine qua non*. A problem is the development of proper criteria for mesh refinement in inelastic, non-standard continua. Although necessary this will probably not prove an easy task.
- There are still open questions with respect to the important issues of stability and uniqueness. This holds *a fortiori* for frictional solids, where we usually have a non-symmetric tangential relationship between the stress and strain tensors[5]. Here a robust algorithm for the numerical determination of bifurcation points and the continuation on the steepest, most critical post-bifurcation branch is not yet available.

ACKNOWLEDGEMENTS

Financial support by CUR-committee A30 'Concrete Mechanics' and by the Commission of the European Communities through the Brite-Euram Programme (Project BE-3275) is gratefully acknowledged.

REFERENCES

1 Aifantis, E.C. On the microstructural original of certain inelastic models, *J. Eng. Mat. Technol.*, **106**, 326–334 (1984)
2 Bazant, Z.P. and Pijaudier-Cabot, G. Nonlocal continuum damage, localization instability and convergence, *J. Appl. Mech.*, **55**, 287–293 (1988)
3 Bazant, Z.P. and Lin, F.-B. Non-local yield limit degradation, *Int. J. Num. Meth. Eng.*, **26**, 1805–1823 (1988)
4 Benallal, A., Billardon, R. and Geymonat, G. Localization phenomena at the boundaries and interfaces of solids, in *Proc. Third Int. Conf. Constitutive Laws for Engineering Materials: Theory and Applications*, (Ed. C.S. Desai), pp. 387–390, Tucson, Arizona (1991)
5 Borst, R. de, Non-linear analysis of frictional materials, *Dissertation*, Delft University of Technology (1986)
6 Borst, R. de, Stability and uniqueness in numerical modelling of concrete structures, *IABSE Rep.*, **54**, 161–176 (1987)
7 Borst, R. de, Numerical methods for bifurcation analysis in geomechanics, *Ing.-Arch.*, **59**, 160–174 (1989)
8 Borst, R. de, Simulation of strain localization: a reappraisal of the Cosserat continuum, *Eng. Comput.*, **8**, 317–332 (1991)
9 Borst, R. de, Numerical modelling of bifurcation and localisation in cohesive-frictional materials, *PAGEOPH*, **137**, 367–390 (1991)
10 Borst, R. de and Sluys, L.J. Localisation in a Cosserat continuum under static and dynamic loading conditions, *Comp. Meth. Appl. Mech. Eng.*, **90**, 805–827 (1991)
11 Borst, R. de, Huerta, A. and Pijaudier-Cabot, G. Localization limiters: properties, implementation and solution control, *TU-Delft Report 25-2-91-2-09* (1991)
12 Borst, R. de, A generalisation for J_2-flow theory for polar continua, *Comp. Meth. Appl. Mech. Eng.*, (1993) to appear
13 Borst, R. de and Mühlhaus, H.-B. Gradient-dependent plasticity: formulation and algorithmic aspects, *Int. J. Num. Meth. Eng.*, **35**, 521–539 (1992)
14 Coleman, B.D. and Hodgdon, M.L. On shear bands in ductile materials, *Arch. Ration. Mech: Anal.*, **90**, 219–247 (1985)
15 Cosserat, E. and Cosserat, F. *Théorie des Corps Deformables*, Herman et fils, Paris (1909)
16 Drucker, D.C. A definition of stable inelastic materials, *J. Appl. Mech.*, **26**, 101–106 (1959)
17 Feenstra, P.H., Borst, R. de and Rots, J.G. Numerical study on crack dilatancy. I: Models and stability analysis, *ASCE J. Eng. Mech.*, **117**, 733–753 (1991)
18 Hill, R. A general theory of uniqueness and stability in elastic-plastic solids, *J. Mech. Phys. Solids*, **6**, 236–249 (1958)
19 Hill, R. Acceleration waves in solids, *J. Mech. Phys. Solids*, **10**, 1–16 (1962)
20 Knowles, J.K. and Sternberg, E. On the failure of ellipticity and the emergence of discontinuous deformation gradients in plane finite elastostatics, *J. Elasticity*, **8**, 329–379 (1978)
21 Koiter, W.T. On the thermodynamic background of elastic stability theory, in *Problems of Hydrodynamics and Continuum Mechanics*, SIAM, Philadelphia, pp. 423–433 (1969)
22 Kratochvil, J. Dislocation pattern formation in metals, *Revue Phys. Appl.*, **23**, 419–429 (1988)
23 Kubin, L.P. and Lépinoux, J. The dynamic organization of dislocation structures, in *Proc. Eighth Int. Conf. on Strength of Metals and Alloys, Tampere*, pp. 35–59 (1988)
24 Lasry, D. and Belytschko, T. Localization limiters in transient problems, *Int. J. Solids Structures*, **24**, 518–597 (1988)
25 Loret, B. and Prévost, J.H. Dynamic strain localization in fluid-saturated porous media, *ASCE J. Eng. Mech.*, **117**, 907–922 (1991)
26 Maier, G. and Hueckel, T. Nonassociated and coupled flow rules of elastoplasticity for rock-like materials, *Int. J. Rock Mech. Min. Sci. Geomech. Abstr.*, **16**, 77–92 (1979)
27 Mier, J.G.M. van, Mode-I fracture of concrete: discontinuous crack growth and crack interface grain bridging, *Cement Concr. Res.*, **21**, 1–15 (1991)
28 Mühlhaus, H.-B. and Vardoulakis, I. The thickness of shear bands in granular materials, *Geotechnique*, **37**, 271–283 (1987)
29 Mühlhaus, H.-B. Continuum models for layered and blocky rock, in *Comprehensive Rock Engineering, Vol. 2: Analysis & Design Methods*, Pergamon Press, Oxford (1993)
30 Mühlhaus, H.-B., Borst, R. de and Aifantis, E.C. Constitutive models and numerical analyses for inelastic materials with microstructure, in *Computer Methods and Advances in Geomechanics* (Eds. G. Beer, J.R. Booker and J.P. Carter), Balkema, Rotterdam and Boston, pp. 377–386 (1991)
31 Mühlhaus, H.-B. and Aifantis, E.C. A variational principle for gradient plasticity, *Int. J. Solids Structures*, **28**, 845–858 (1991)
32 Nagtegaal, J.C., Parks, D.M. and Rice, J.R. On numerically accurate finite element solutions in the fully plastic range, *Comp. Meth. Appl. Mech. Eng.*, **4**, 153–177 (1974)

33 Needleman, A. and Tvergaard, V. Finite element analysis of localization in plasticity, in *Finite Elements: Special Problems in Solid Mechanics* (Eds. J.T. Oden and G.F. Carey), Prentice-Hall, Englewood Cliffs, NJ, pp. 94–157 (1984)
34 Needleman, A. Material rate dependence and mesh sensitivity in localization problems, *Comp. Meth. Appl. Mech. Eng.*, **67**, 69–86 (1988)
35 Needleman, A. and Ortiz, M. Effect of boundaries and interfaces on shear-band localization, *Int. J. Solids Structures*, **28**, 859–878 (1991)
36 Ortiz, M., Leroy, Y. and Needleman, A. A finite element method for localization in failure analysis, *Comp. Meth. Appl. Mech. Eng.*, **61**, 189–214 (1987)
37 Pamin, J. and Borst, R. de, A rectangular element for gradient plasticity, in *Computational Plasticity: Fundamentals and Applications* (Eds. D.R.J. Owen, E. Onate and E. Hinton), Pineridge Press, Swansea, pp. 2009–2020 (1992)
38 Pijaudier-Cabot, G. and Bazant, Z.P. Nonlocal damage theory, *ASCE J. Eng. Mech.*, **113**, 1512–1533 (1987)
39 Rots, J.G., Nauta, P., Kusters, G.M.A. and Blaauwendraad, J. Smeared crack approach and fracture localization in concrete, *HERON*, **30**, (1), 1–48 (1984)
40 Rudnicki, J.W. and Rice, J.R. Conditions for the localization of deformation in pressure-sensitive dilatant solids, *J. Mech. Phys. Solids*, **23**, 371–394 (1975)
41 Schaefer, H. Versuch einer Elastizitätstheorie des zweidimensionalen ebenen Cosserat-Kontinuums, in *Miszellaneen der Angewandten Mechanik* (Ed. M. Schäfer), Akademie-Verlag, Berlin, pp. 277–292 (1962)
42 Schreyer, H.L. and Chen, Z. One-dimensional softening with localization, *J. Appl. Mech.*, **53**, 791–979 (1986)
43 Shawki, T.G. and Clifton, R.J. Shear-band formation in thermal viscoplastic materials, *Mech. Mat.*, **8**, 13–43 (1989)
44 Simo, J.C. Strain softening and dissipation : a unification of approaches, in *Cracking and Damage: Strain Localization and Size Effect* (Eds. J. Mazars and Z.P. Bazant), Elsevier, New York, pp. 440–461 (1989)
45 Sluys, L.J. and Borst, R. de, Rate-dependent modelling of concrete fracture, *HERON*, **36**, (2), 1–15 (1991)
46 Sluys, L.J., Borst, R. de and Mühlhaus, H.-B. Wave propagation and localisation in a gradient-dependent elastic-plastic solid, in *Nonlinear Engineering Computations* (Eds. N. Bićanić *et al.*), Pineridge Press, Swansea, pp. 287–297 (1991)
47 Sluys, L.J. Wave propagation, localisation and dispersion in softening solids, *Dissertation*, Delft University of Technology (1992)
48 Sluys, L.J., Bolck, J. and Borst, R. de, Wave propagation and localisation in visco-plastic media. *Computational Plasticity: Fundamentals and Applications* (Eds. D.R.J. Owen, E. Onate and E. Hinton), Pineridge Press, Swansea, pp. 539–550 (1992)
49 Sluys, L.J. and Borst, R. de, Wave propagation and localisation in a rate-dependent cracked medium: model formulation and one-dimensional examples, *Int. J. Solids Structures*, **29**, 2945–2950 (1992)
50 Steinmann, P. and William, K. Performance of enhanced finite element formulations in localized failure computations, *Comp. Meth. Appl. Mech. Eng.*, **90**, 845–867 (1991)
51 Walgraef, D. and Aifantis, E.C. On the formation and stability of dislocation patterns, I–III, *Int. J. Eng. Sci.*, **12**, 1351–1372 (1985)
52 William, K. Failure assessment of the extended Leon model for plain concrete, in *Proc. 2nd Int. Conf. Computer Aided Analysis and Design of Concrete Structures* (Eds. N. Bićanić and H.A. Mang), Pineridge Press, Swansea, pp. 851–865 (1990)
53 Wu, F.H. and Freund, L.B. Deformation trapping due to thermoplastic instability in one-dimensional wave propagation, *J. Mech. Phys. Solids*, **32**, 119–132 (1984)